



Coupling of the triplet states of a negatively charged exciton in a quantum dot with the spin of a magnetic atom

L. Besombes ^{1,2,*}, S. Ando,³ S. Kuroda ^{3,2} and H. Boukari¹

¹*Institut Néel, CNRS, Université Grenoble Alpes, and Grenoble INP, 38000 Grenoble, France*

²*Japanese-French Laboratory for Semiconductor Physics and Technology (J-FAST)–CNRS–Université Grenoble Alpes–Grenoble INP–University of Tsukuba, 1-1-1 Tennoudai, Tsukuba 305-8573, Japan*

³*Institute of Materials Science, University of Tsukuba, 1-1-1 Tennoudai, Tsukuba 305-8573, Japan*



(Received 31 March 2023; revised 1 June 2023; accepted 14 June 2023; published 26 June 2023)

Two electrons in a quantum dot (QD) can form triplet states. We analyze the exchange coupling of the triplet states of the negatively charged exciton in a QD (X^- , two electrons and one hole) with the spin of a magnetic atom (Mn). Two techniques are used to access the spin structure of this magnetic complex: the resonant excitation of the excited states of X^- -Mn and the analysis of the emission of a negatively charged biexciton in a magnetic dot (XX^- -Mn). The photoluminescence (PL) excitation of X^- -Mn reveals excited states with a circularly polarized fine structure which strongly depends on the Mn spin state S_z and gives rise to negative circular polarization emission. This fine structure arises from the coupling of the triplet states of an excited charged exciton with the Mn atom (X^{*-} -Mn), and its S_z dependence can be described by a spin effective model. The recombination of XX^- -Mn leaves in the dot a charged exciton in its excited state, and the PL structure is controlled by the coupling of triplet states of X^{*-} with the Mn spin. An analysis of the polarization and magneto-optic properties of this emission gives access to the electron-hole exchange interaction within the triplet states. Comparing the fine structures of the singlet X^- -Mn and of the triplets of X^{*-} -Mn, we can independently study the different sources of anisotropy in the QD: the valence band mixing and the exchange interaction in an anisotropic potential.

DOI: [10.1103/PhysRevB.107.235305](https://doi.org/10.1103/PhysRevB.107.235305)

I. INTRODUCTION

The spin state of a carrier in a semiconductor quantum dot (QD) or of an individual impurity in a semiconductor host can act as a bit of quantum information. The transfer of quantum information between such solid-state quanta and single photons is extensively studied as it is an essential element towards the establishment of quantum information networks [1]. Optically active semiconductor QDs can be key systems for spin-photon quantum coupling [2] as in a QD containing a single carrier, the polarization of the optical emission is directly linked to the spin of the resident carrier.

Confined carriers in QDs can be exchange coupled with embedded magnetic elements. This exchange interaction can be exploited to transfer information between the spin of carriers, proposed as efficient qubits in quantum computing devices [3,4], and a more localized spin on a defect or an impurity. In the case of an optically active QD, this exchange coupling also provides optical access to a strongly localized spin. This has been demonstrated for some transition-metal elements in II-VI and III-V semiconductors [5–14] and could be extended to other nonoptically active individual magnetic defects.

The optical selection rules and the spin dynamics in QDs are strongly influenced by the electron-hole (e-h) exchange interaction. In the three-dimensional confinement potential of

a dot, the exchange interaction intensifies and usually become anisotropic. This is observed in neutral QDs where an exchange interaction of electron and hole induced by a dot asymmetry splits the exciton radiative doublet and destroys the spin polarization of QD excitons [15].

The e-h exchange interaction is absent for the singlet (S_0) of a negatively charged exciton (X^- , also called a negative trion) in the ground state of a QD. However, when at least an electron occupies an excited state of the dot, the two electrons of X^- form triplet states ($T_0, T_{\pm 1}$). Electron-electron (e-e) and e-h exchange interactions partly remove the spin degeneracy of these triplets. The spin dynamics among the triplets is dominated by the e-h exchange interaction and is at the origin of the negative circular polarization in the photoluminescence (PL) of negatively charged QDs [16–19]. The negative circular polarization rate depends on the spin of the resident electron and is a probe of possible optical pumping of the electron spin interacting with the nuclear spin bath of the semiconductor host [20,21].

The presence of a transition-metal element in the QD significantly modifies the spin structure as both the electrons and the holes are coupled with the localized spin of the magnetic atom through the $sp-d$ exchange interaction [22]. This exchange interaction permits, in particular, the spin of the atom to be interfaced with single photons. In the case of a singly charged dot, it has been shown that the simple unpolarized single-line emission of a charged exciton transforms into an 11-line spectrum in the presence of a single Mn atom. This has been demonstrated both for X^- [23,24] and

*lucien.besombes@neel.cnrs.fr

X^+ [25,26]. Whereas triplets of two unpaired electrons in self-assembled or electrostatic QDs have been extensively studied [18–21,27–30], the structure and the spin dynamics of such triplet states coupled with a magnetic impurity have not been investigated.

In this paper, we analyze how the triplet states of two electrons couple with the spin of a magnetic atom. We first investigate the exchange coupling of excited negatively charged excitons (X^{-*}) with a Mn atom ($S = 5/2$) in a CdTe/ZnTe QD and analyze how the spin relaxation mechanism of the triplets is affected by the exchange interaction with the Mn spin. PL excitation (PLE) spectra of X^- coupled with a Mn atom (X^- -Mn) exhibits resonances with circularly polarized fine structure arising from a direct excitation of triplet states exchange coupled with the Mn spin. The splitting of these absorption resonances depends on the spin state S_z of the magnetic atom. The direct injection of spin-polarized e-h pairs on the excited states can give rise to large cross-circularly-polarized emission. A model of the circularly polarized fine structure of the PLE is presented.

In some of the charged dots, the emission of the negatively charged biexciton coupled with the Mn (XX^- -Mn) is observed. It can be used as a monitor of the optically active triplet states of X^{-*} -Mn as they are left behind after the optical recombination of the complex. Its linear polarization and magneto-optical properties are analyzed. In particular, the PL of XX^- -Mn permits us to observe both the isotropic and the anisotropic parts of the e-h exchange interaction within the triplets. Different directions of linear polarization are usually observed in the fine structure of X^- -Mn and XX^- -Mn. This shows the independence between the principal axis of the strain-induced valence band mixing (VBM) and the shape anisotropy of the dots. The linearly polarized fine structure and the magnetic field dependence of XX^- -Mn can be modeled by a spin effective Hamiltonian. A slight reduction of the anisotropic part of the e-h exchange interaction is observed under a magnetic field applied along the QD growth axis.

The rest of the paper is organized as follows. After a short presentation of the sample and experiments in Sec. II, we discuss in Sec. III the PL of negatively charged Mn-doped QDs where the emission of charged excitons and charged biexcitons can be identified. In Sec. IV, we analyze the circularly polarized fine structure of the resonantly excited triplet states of X^- coupled with the spin of a Mn atom. In Sec. V we discuss the magneto-optics properties of the XX^- coupled with a magnetic atom and show how they can be used to access the structure of the excited charged exciton triplet.

II. SAMPLES AND EXPERIMENTAL SETUP

In this paper we use self-assembled CdTe/ZnTe QDs grown by molecular beam epitaxy and doped with Mn atoms. The growth method and structure of these dots were presented in Ref. [31]. The concentration of Mn is adjusted to obtain QDs containing 0, 1, or a few magnetic atoms. n -type doping with aluminum is introduced in the capping layer 30 nm away from the QD layer. When doped with a single magnetic atom, these dots permit us to optically access the spin of a Mn atom interacting with negatively charged excitonic complexes.

Individual QDs are studied by optical microspectroscopy at liquid helium temperature ($T = 4.2$ K). The sample is mounted in x , y , z piezo actuators and inserted in a vacuum tube under a low pressure of He exchange gas. The tube is immersed in the variable-temperature insert of the cryostat filled with liquid He. The sample temperature is measured thanks to a sensor located in the copper sample holder. The cryostat is equipped with a vectorial superconducting coil, and a magnetic field up to 9 T along the QD growth axis and 2 T in the QD plane can be applied.

The PL is excited with a tunable dye laser (Coherent CR599 with rhodamine 6G) and collected by a high-numerical-aperture microscope objective ($NA = 0.85$). For spectral analysis, the PL is dispersed by a 2-m double-grating spectrometer (1800 lines/mm) and detected by a cooled Si charge-coupled device (CCD; Andor Newton).

A half-wave plate in front of a linear polarizer is used to analyze the linear polarization. For circular polarization measurement, a quarter-wave plate oriented at 45° from the linear polarization direction of the excitation laser is introduced in the excitation and detection path. The half-wave plate and linear polarizer are then used to select cocircularly- or cross-circularly-polarized PL. For the PLE measurements, the power of the tunable dye laser is stabilized with an electro-optic variable attenuator.

III. PL OF NEGATIVELY CHARGED Mn-DOPED QDs

The typical emissions of negatively charged Mn-doped QDs are presented in Fig. 1. They present a complex PL spectrum which strongly depends on the excitation power. However, among these emission lines, the PL of the ground state of X^- -Mn can be identified at zero magnetic field by (i) the number of PL lines and (ii) the linear polarization dependence of the PL (see, for instance, QD1 in Fig. 1) [23,24,26]. Let us first recall here the origin of this PL structure for X^- -Mn. This will also be used in the next sections to model the resonant excitation of the charged exciton triplet states and will help us to understand the PL properties of the negatively charged biexciton coupled with a Mn spin.

The emitting state of X^- -Mn has two electrons and one hole coupled to the Mn spin. The effect of the two spin-paired electrons on the Mn can be neglected, and X^- -Mn is governed by the hole-Mn interaction $\mathcal{H}_{h-Mn} = I_{h1Mn} \vec{S} \cdot \vec{J}$. I_{h1Mn} is the exchange integral of a hole located in the ground state of the dot with the Mn spin. In the heavy-hole approximation the 12 eigenstates of $\mathcal{H}_{h-Mn} = I_{h1Mn} S_z J_z$, $|S_z, J_z\rangle$, with z along the QD growth axis, are organized as six doublets with defined S_z and J_z [23,26].

In the subspace of the two low-energy heavy-hole states $J_z = \pm 3/2$, a pseudospin operator \tilde{j} can be used to take into account a possible VBM [32,33]. For a VBM induced by an in-plane anisotropy of the strain, the components of \tilde{j} are related to the Pauli matrices τ by $\tilde{j}_z = \frac{3}{2}\tau_z$ and $\tilde{j}_\pm = -2\sqrt{3}e^{-2i\theta_s}\rho_s/\Delta_{lh}\tau_\pm$. ρ_s is the coupling energy between heavy holes and light holes split by the energy Δ_{lh} , and θ_s is the angle relative to the [100] axis of the principal axis of the anisotropy responsible for the VBM.

Recombination of one of the electrons with the hole leaves a final state with an electron coupled to the Mn atom by

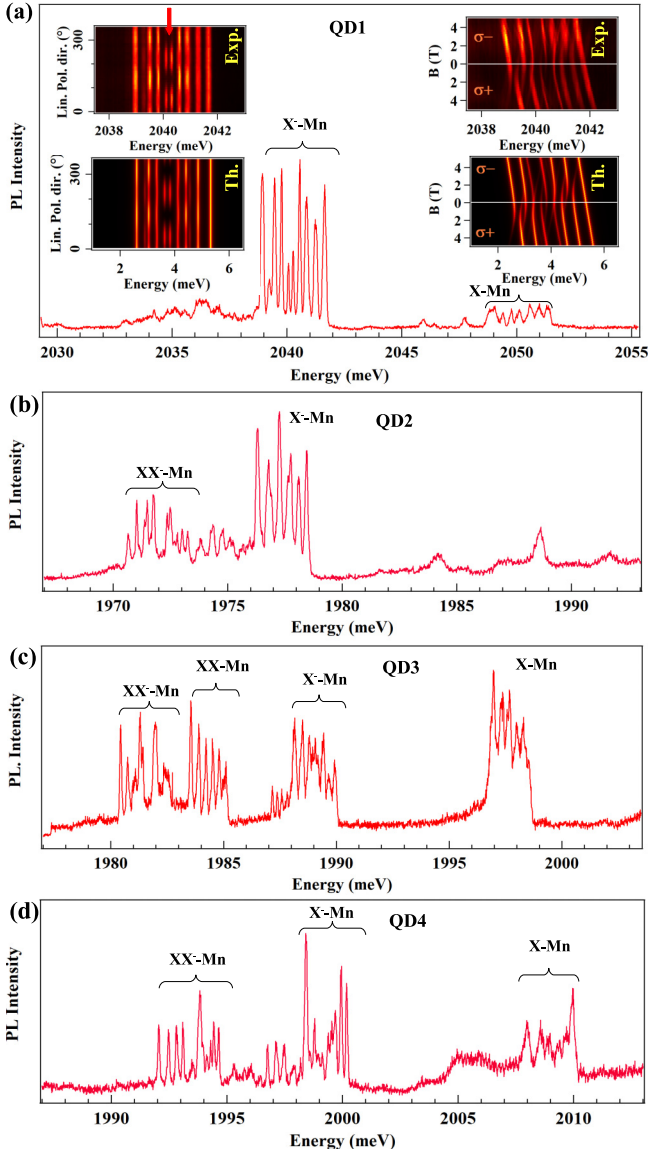


FIG. 1. PL of QDs in a negatively charged Mn-doped sample. QD1 ($E_{\text{ex}} = 2102$ meV) (a) is dominated by X^- -Mn. Its linearly polarized structure is presented in the left insets (angles are in degrees, and 0° corresponds to either the [100] or [010] axis), and its magnetic field dependence is presented in the right insets (yellow corresponds to a maximum of intensity). Additional PL lines can appear on the low-energy side of the X^- -Mn: See XX^- -Mn and XX^- -Mn in QD2 ($E_{\text{ex}} = 2079$ meV) (b), QD3 ($E_{\text{ex}} = 2077$ meV) (c), and QD4 ($E_{\text{ex}} = 2074$ meV) (d). The parameters used in the model are $I_{e_1\text{Mn}} = -100$ μeV , $I_{h_1\text{Mn}} = 320$ μeV , $\rho_s/\Delta_{lh} = 0.15$, $\theta_s = \pi/4$, $g_e = -0.4$, $g_h = 0.5$, and $g_{\text{Mn}} = 2$. A line broadening with a Lorentzian of half width at half maximum of 50 μeV is included. Lin. pol. dir., linear polarization direction; Exp., experimental; Th., theoretical.

$\mathcal{H}_{e\text{-Mn}} = I_{e_1\text{Mn}} \vec{S} \cdot \vec{\sigma}$. $I_{e_1\text{Mn}}$ is the exchange integral of the electron in the ground state with the Mn atom. The 12 eigenstates of the electron-Mn complex are split into a ground state septuplet (total spin $M = 3$) and a higher energy level with $M = 2$ (degeneracy of 5) [23]. We label them all as $|M, M_z\rangle$.

For each of the six levels of X^- -Mn there are two possible final states with either $M = 2$ or $M = 3$. The Mn spin is not affected by the optical transition, and the weight of the transitions is given by both optical and spin conservation rules. We consider, for instance, a $\sigma+$ transition where the $|\downarrow_1, \uparrow_1\rangle$ e-h pair is annihilated. After the recombination, the resulting state is $|S_z, \uparrow_1\rangle$. The intensity of the optical transition from an initial state $|\uparrow_1, \downarrow_1\rangle \times |S_z, \uparrow_1\rangle$ is proportional to the overlap $\langle M, M_z | S_z, \uparrow_1 \rangle$ (the Clebsch-Gordan coefficient of the composition of a spin 1/2 with a spin 5/2).

The highest-energy transition corresponds to the high-energy initial state $|\uparrow_1, \downarrow_1\rangle \times |5/2, \uparrow_1\rangle$ and to the final state $|5/2, \uparrow_1\rangle$ which is identical to $|3, +3\rangle$ and gives the highest optical weight. Transition to the final state $|2, M_z\rangle$, which does not contain any $|5/2, \uparrow_1\rangle$ component, is forbidden. The other five doublets have optical weights between 1/6 and 5/6 with both $|2, M_z\rangle$ and $|3, M_z\rangle$ final states, and the number of resolved lines is 11 [23,24,26].

A linear polarization map of the PL of X^- -Mn is presented for QD1 in Fig. 1(a). Linearly polarized lines [indicated by an arrow in the upper left inset of Fig. 1(a)] are observed slightly shifted to the low-energy side of the center of the structure. They arise from spin-flip interaction between the Mn atom and the hole induced by the presence of VBM [23]. Provided that $\rho_s/\Delta_{lh} \ll 1$, the effect of this interaction is small on all the h-Mn doublets except for the states $|-1/2, \uparrow_1\rangle$ and $|+1/2, \downarrow_1\rangle$ which are initially degenerated. Combinations of these states are coupled, via linearly polarized photons, to the $|2, 0\rangle$ and $|3, 0\rangle$ electron-Mn states. Polarization directions are controlled by the strain in the QD plane through the Bir-Pikus Hamiltonian which describes the valence band structure [34].

We can obtain numerical values of $I_{h_1\text{Mn}}$, $I_{e_1\text{Mn}}$, and ρ_s/Δ_{lh} comparing the transition probabilities calculated from a diagonalization of $\mathcal{H}_{h\text{-Mn}}$ and $\mathcal{H}_{e\text{-Mn}}$ with the experimental data [left insets of Fig. 1(a)]. A VBM is observed in most of the QDs, but the value of the coefficient ρ_s/Δ_{lh} shows that the hole-Mn exchange interaction remains highly anisotropic (dominant heavy-hole character). These parameters can be confirmed by an analysis of the magnetic field dependence of the emission. A longitudinal magnetic field dependence is presented in the upper right inset of Fig. 1(a) and compared with the result of the modeling with the same parameters as the ones used to calculate the linear polarization map at zero field.

Under high excitation power, additional emission multiplets usually appear on the low-energy side of X^- -Mn (see QD2, QD3, and QD4 in Fig. 1). As we discuss in Sec. V, they correspond to neutral and charged biexcitons interacting with the Mn spin.

IV. EXCITED STATES IN NEGATIVELY CHARGED Mn-DOPED QDs

Let us first focus on the optical properties of the singly charged exciton. PLE spectra of X^- -Mn are presented in Fig. 2 for two QDs: QD1, which presents a large ground state exchange splitting, and QD5, with a weaker splitting. For both QDs, absorption resonances in the PLE spectra are observed on top of an absorption background. For a cross-linear excita-

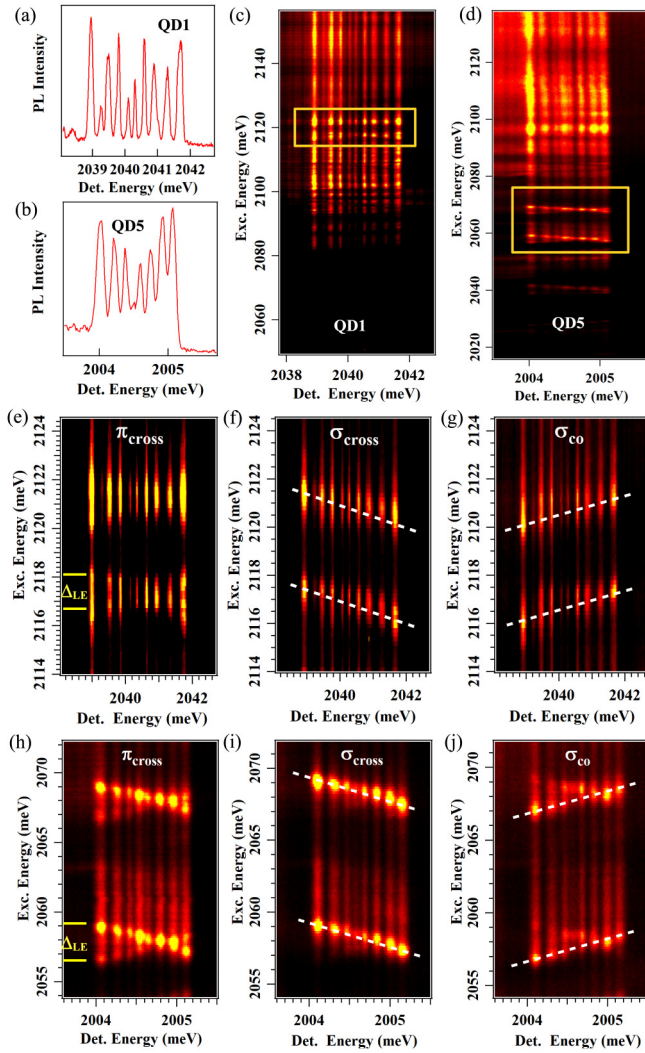


FIG. 2. Polarized fine structure of the excited states in two negatively charged Mn-doped QDs, QD1 with a large X^- -Mn splitting and QD5 with a smaller splitting. (a) and (b) present the PL of X^- -Mn in QD1 ($E_{ex} = 2102$ meV) and QD5 ($E_{ex} = 2097$ meV), respectively. (c) and (d) are PLE intensity maps in the π_{cross} excitation and detection configuration for QD1 and QD5, respectively. (e), (f), and (g) present details of the PLE of QD1 for the excited states highlighted in (c) in the π_{cross} , σ_{cross} , and σ_{co} configurations, respectively. (h), (i), and (j) present details of the PLE of QD5 for the excited states highlighted in (d) in the π_{cross} , σ_{cross} , and σ_{co} configurations, respectively. In the PL maps, yellow corresponds to a maximum of intensity. Det., detection; Exc., excitation.

tion and detection configuration (π_{cross}), absorption structures with an asymmetric-cross-like shape are observed in the PLE intensity maps [see details in Fig. 2(e) for QD1 and Fig. 2(h) for QD5].

When spin-polarized e-h pairs are injected through circularly polarized photoexcitation on excited states, the PLE spectra reveal resonances with a strong circular polarization dependence. This is illustrated in Figs. 2(f) and 2(g) for QD1 and Figs. 2(i) and 2(j) for QD5. The co-circularly-polarized (σ_{co}) and the cross-circularly-polarized (σ_{cross}) PLE intensity maps clearly show a different excitation energy dependence

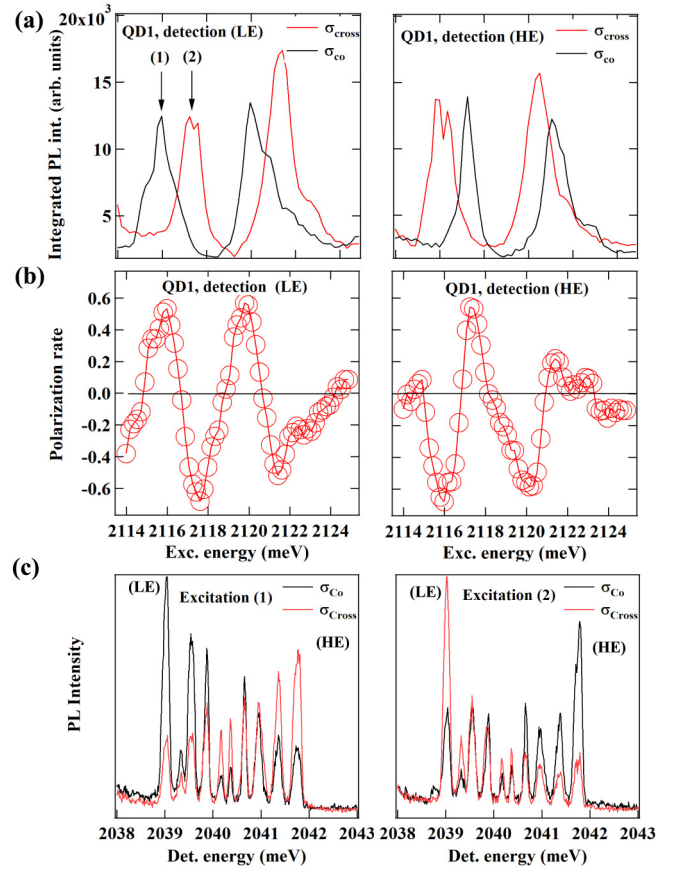


FIG. 3. (a) Circularly polarized PLE spectra of X^- -Mn in QD1 for a detection on the low-energy (LE) line (left panel) and on the high-energy (HE) line (right panel). (b) Corresponding circular polarization rate. (c) Circularly polarized PL spectra obtained for a resonant excitation: excitation (1) (left panel) and excitation (2) (right panel). The low-energy and the high-energy PL lines are labeled by “LE” and “HE,” respectively. Here, int., intensity.

with a positive slope in σ_{co} [i.e., low-energy excitation gives a PL on the low-energy (LE) line, and high-energy excitation gives a PL on the high-energy (HE) line] and a negative slope in σ_{cross} (i.e., low-energy excitation gives a PL on the HE line, and high-energy excitation gives a PL on the LE line). The observation of strongly circularly polarized emission (either σ_{co} or σ_{cross}) shows first that the spin of the hole-Mn complex is well conserved during the lifetime of X^- .

For each line of X^- -Mn, PLE resonances displaying a fine structure doublet are resolved in the circularly polarized PLE maps. This is particularly clear on the HE and LE lines. For instance, as detailed for QD1 in Fig. 3, a switching between positive and negative circular polarization rate is observed as the laser excitation energy is increased around the excited states at 2116 and 2121 meV.

The splitting of the observed absorption doublet depends on the X^- -Mn line. In particular, as shown in Fig. 3(a), the order of circularly polarized PLE resonances is reversed for detection on the LE line [Fig. 3(a), left panel] and for detection on the HE line [Fig. 3(a), right panel]. For detection on the LE line when the excitation energy is increased, the σ_{co} emission

is first observed. The order is reversed for a detection on the HE line, where the σ_{cross} PL appears first. For a detection in the center of the PL spectra, the two absorption resonances are usually not resolved in the PLE spectra.

Such a doublet structure with a circular polarization reversal can usually be observed on different excited states of X^- -Mn. The measured splitting is changing from one excited state to another and from dot to dot. This is illustrated, for instance, by a comparison of excited states in QD1 and QD5. Whereas the splitting between the σ_{co} and σ_{cross} PLE resonances measured on the low-energy line $\Delta_{\text{LE}} \approx 1.4$ meV on QD1 [Fig. 2(e)], a much larger value is observed on QD5 with $\Delta_{\text{LE}} \approx 2.2$ meV [Fig. 2(h)]. QD5, with the smallest carrier-Mn exchange interaction in the ground state of X^- -Mn, presents the largest splitting in the excited state doublets.

A. The triplet states of the charged exciton coupled with a Mn spin

To understand this circularly polarized structure in the PLE, one has to consider that the optical injection of an e-h pair on an excited state of a negatively charged QD creates an excited negatively charged exciton, X^{*-} -Mn. It consists of a resident electron in the ground state of the dot and an e-h pair in the resonantly addressed excited state.

For a sufficiently large confinement of the carriers on the excited state, the e-e and the e-h exchange interactions induce a fine structure of X^{*-} -Mn (Fig. 4). In a nonmagnetic dot, the strongest term is the e-e exchange interaction, which reduces in a spherical approximation to a Heisenberg Hamiltonian [28]:

$$H_{e_1, e_2} = \Delta^{ee} \vec{\sigma}_1 \cdot \vec{\sigma}_2, \quad (1)$$

where $\vec{\sigma}_1$ ($\vec{\sigma}_2$) is the spin operator of the electron on the ground (excited) state and $\Delta^{ee} < 0$ is the exchange integral. This Hamiltonian splits the excited singlet of the two electrons S_0^* with total angular momentum $I = 0$ (where $I = \sigma_1 + \sigma_2$) from the lower-energy triplet states T_0 , $T_{\pm 1}$ with $I = 1$ and $I_z = 0, \pm 1$. This splitting is typically equal to a few meV for an electron on an excited state of InAs/GaAs self-assembled QDs [18,19] and could be larger in II-VI compounds presenting a larger Coulomb interaction.

Within X^{*-} , the e-h exchange interaction Δ^0 is a smaller correction (typically a few hundred μeV [21]) which splits the triplet states [see Fig. 4(a)]. The two electrons are coupled to each other much more strongly than each of them is coupled to the hole. One can then consider the exchange interaction of the three particles as an interaction of the hole spin with the total spin of the two electrons $I = \sigma_1 + \sigma_2$. This e-h exchange interaction can be written in a compact form [29]:

$$H_{e_1 e_2 h_2} = 2\tilde{\Delta}^0 I_z \sigma_z^h + \tilde{\Delta}^1 (I_x \sigma_x^h + I_y \sigma_y^h) \quad (2)$$

with $\sigma_i^h = 1/2\tau_i$ (with τ_i being the Pauli matrices) acting on the heavy-hole subspace. $\Delta^{0,1} = 1/2(\Delta_1^{0,1} + \Delta_2^{0,1})$ is an average of the hole exchange interaction with the electron on the ground ($\Delta_1^{0,1}$) and excited ($\Delta_2^{0,1}$) state. The second term in (2) is an effective description of the long-range part of the e-h exchange interaction which becomes nonzero in an anisotropic confinement potential [32,35].

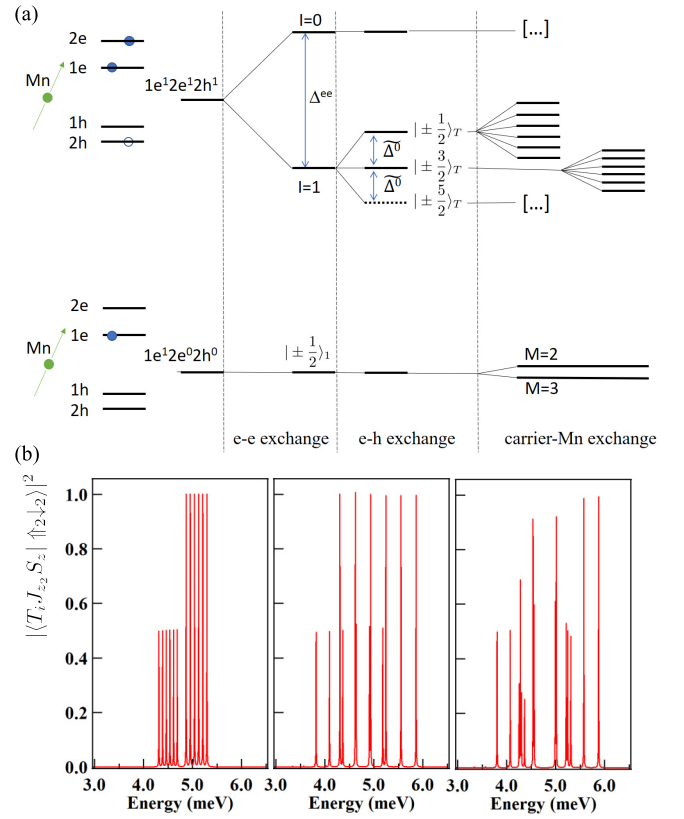


FIG. 4. (a) Scheme of the energy levels of a resonantly created X^{*-} -Mn. (b) Calculated energy levels of the X^{*-} triplet states interacting with a Mn spin. The intensity gives the bright exciton ($\sigma+$) component, and only the bright triplets appear. The parameters used in the calculation are as follows: $I_{e_2 \text{Mn}} = 0$ μeV , $\Delta^{ee} = -5000$ μeV , $\tilde{\Delta}^0 = -580$ μeV , $\rho_s / \Delta_{lh} = 0$, $\theta_s = 0$, and (left panel) $I_{e_1 \text{Mn}} = -30$ μeV , $I_{h_2 \text{Mn}} = 50$ μeV , and $\tilde{\Delta}^1 = 0$ μeV ; (center panel) $I_{e_1 \text{Mn}} = -80$ μeV , $I_{h_2 \text{Mn}} = 180$ μeV , and $\tilde{\Delta}^1 = 0$ μeV ; and (right panel) $I_{e_1 \text{Mn}} = -80$ μeV , $I_{h_2 \text{Mn}} = 180$ μeV , and $\tilde{\Delta}^1 = 250$ μeV .

In the case of a simple e-h pair in the QD ground state, this effective spin Hamiltonian with $\tilde{\Delta}^0 < 0$ stabilizes the states with parallel electron and hole spins (separates high energy radiative excitons and low energy nonradiative excitons) and splits the high-energy radiative exciton with the energy $\tilde{\Delta}^1$ (the usual fine structure splitting of the exciton).

In the case of X^{*-} , this e-h exchange interaction splits the electron triplet states [27,29]. According to Ref. [27], the charged exciton states read

$$\begin{aligned} |\pm \frac{1}{2}\rangle_T &= T_{\mp 1} |\pm \frac{3}{2}\rangle_2 = (|\mp \frac{1}{2}\rangle_1 |\mp \frac{1}{2}\rangle_2) |\pm \frac{3}{2}\rangle_2, \\ |\pm \frac{3}{2}\rangle_T &= T_0 |\pm \frac{3}{2}\rangle_2 = \frac{1}{\sqrt{2}} (|\pm \frac{1}{2}\rangle_1 |\mp \frac{1}{2}\rangle_2 + |\mp \frac{1}{2}\rangle_1 |\pm \frac{1}{2}\rangle_2) |\pm \frac{3}{2}\rangle_2, \\ |\pm \frac{5}{2}\rangle_T &= T_{\pm 1} |\pm \frac{3}{2}\rangle_2 = (|\pm \frac{1}{2}\rangle_1 |\pm \frac{1}{2}\rangle_2) |\pm \frac{3}{2}\rangle_2, \end{aligned} \quad (3)$$

where $|\sigma_z\rangle_i$ ($|J_z\rangle_i$) is the spin state of an electron (hole) on level i . The X^{*-} triplet states ($|\pm \frac{1}{2}\rangle_T$, $|\pm \frac{3}{2}\rangle_T$, $|\pm \frac{5}{2}\rangle_T$) are labeled with their total angular momentum projections along the QD growth axis z . The nondiagonal exchange terms $\tilde{\Delta}^1$ couple the triplet states $T_{-1} |\pm \frac{3}{2}\rangle_2$ and the states $T_0 |\mp \frac{3}{2}\rangle_2$ on one side and $T_{+1} |\mp \frac{3}{2}\rangle_2$ and $T_0 |\pm \frac{3}{2}\rangle_2$ on the other side [27,29]. The $|\pm \frac{5}{2}\rangle_T$

triplet states only contain the e-h component in the excited state with parallel electron and hole spins with an angular momentum ± 2 . They cannot be created by a resonant optical excitation (angular momentum ± 1) and are dark.

In a Mn-doped QD, these split X^{*-} states interact with the spin of the magnetic atom. This can be described by the carrier-Mn spin effective Hamiltonian:

$$H_{X^{*-}\text{-Mn}} = H_{e_1 e_2 h_2} + I_{e_1 \text{Mn}} \vec{\sigma}_1 \vec{S} + I_{e_2 \text{Mn}} \vec{\sigma}_2 \vec{S} + I_{h_2 \text{Mn}} \vec{J}_2 \vec{S}, \quad (4)$$

where $I_{e_i \text{Mn}}$ ($I_{h_i \text{Mn}}$) are the exchange integrals between the electrons (hole) and the Mn spins. The exchange integrals for carriers on excited states depend on the overlap with the magnetic atom and can significantly change from one excited state to another. As for carriers confined in the ground state, the exchange interaction is expected to be dominated by the antiferromagnetic coupling with the hole spin. It can also be affected by a possible VBM.

Calculated energy levels of the triplet states of X^{*-} interacting with a Mn spin are presented in Fig. 4(b). If the exchange interaction with the Mn spin is weaker than the e-h exchange interaction $\tilde{\Delta}_0$, it further splits into six levels the optically active states of X^{*-} [Fig. 4(b), left panel]. The largest splitting is obtained for the highest-energy triplet states $|\pm 1/2\rangle$, where the antiferromagnetic interaction with the hole and ferromagnetic interaction with both electrons add. The splitting of the lower energy states $|\pm 3/2\rangle$ is only controlled by the exchange interaction with the hole spin on the excited state. The lowest-energy triplet is dark and does not appear in Fig. 4(b), which only displays a bright exciton component $|\langle T_i J_z S_z | \uparrow_2 \downarrow_2 \rangle|^2$.

The two bright triplets can overlap if the energy shift induced by the exchange interaction with the Mn is larger than the e-h exchange splitting $\tilde{\Delta}_0$ [Fig. 4(b), center panel]. In the presence of an anisotropic e-h exchange interaction a gap appears in the center of the structure [Fig. 4(b), right panel, around 4.8 meV]. The width of the gap is controlled by $\tilde{\Delta}^1$. This mixing can induce linear polarization in the absorption of the triplets with polarization directions controlled by the shape anisotropy of the wave function in the excited state. Neglecting this possible mixing, each level of the split triplet corresponds to a given spin state S_z of the Mn.

B. Circularly polarized fine structure of the excited states in a charged Mn-doped QD

The optical excitation of an excited state of a charged dot creates a triplet state of $X^{*-}\text{-Mn}$. Independently of its spin, the optically created hole can relax towards the ground state of the dot. For the electron, because of the Pauli exclusion, the relaxation channels are not straightforward and depend on the relative orientation of the resident and injected electrons' spin. For a given Mn spin state S_z , the relaxation of $X^{*-}\text{-Mn}$ towards $X^- \text{-Mn}$ will then depend on the triplet state which is created.

Let us consider, for instance, a $\sigma+$ excitation which creates an e-h pair $|\downarrow_2, \uparrow_2\rangle$ on an excited state of a charged magnetic dot. This e-h pair is exchange coupled with the electron resident on the ground state and the embedded Mn atom. The exchange interaction with the Mn spin is dominated by the

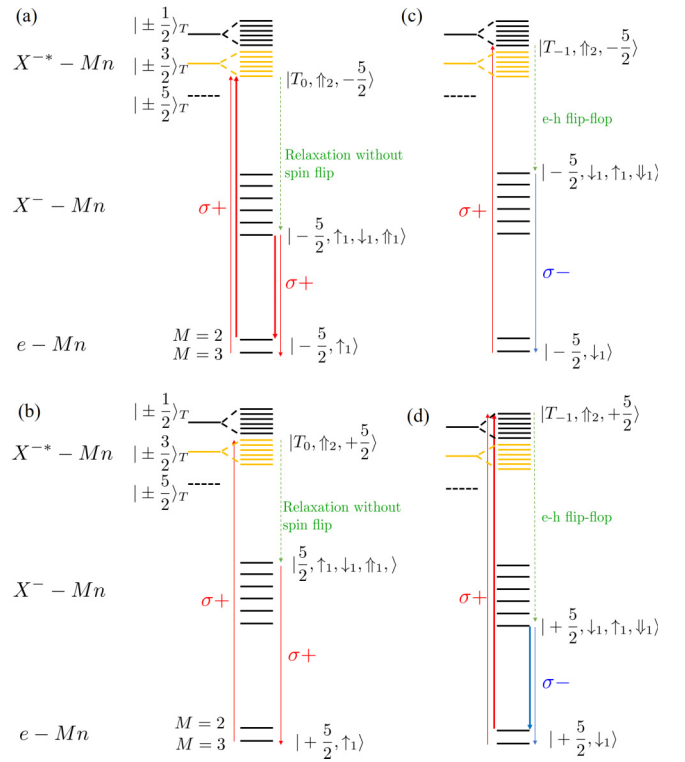


FIG. 5. Path of resonant optical excitation and spin relaxation in a negatively charged Mn-doped QD which contains a spin-up electron $|\uparrow_1\rangle$ [(a) and (b)] or a spin-down electron $|\downarrow_1\rangle$ [(c) and (d)]. Only the cases of resonant excitation on the low and the high energy levels of the split triplet states are presented.

antiferromagnetic coupling with the spin-up hole $|\uparrow_2\rangle$. In a first approximation, the lowest-energy triplet states $|\pm 5/2\rangle_T$ are dark and cannot produce any significant resonance in the PLE spectra.

When a spin-up electron $|\uparrow_1\rangle$ is present in the dot, an absorption can occur on the triplet state $|\pm 3/2\rangle_T$. The lowest-energy triplet state $|T_0, \uparrow_2, -5/2\rangle$ is associated with $S_z = -5/2$ [Fig. 5(a)]. It can be created by an optical transition from the electron-Mn state $|-5/2, \uparrow_1\rangle$. Two transitions are possible from $M = 2$ or $M = 3$. The intensities of the transitions are proportional to $|\langle 2, -2 | -5/2, \uparrow_1 \rangle|^2 = 5/6$ and $|\langle 3, -2 | -5/2, \uparrow_1 \rangle|^2 = 1/6$, respectively. This gives rise to a large intensity transition from $M = 2$ and a higher-energy less intense transition from $M = 3$. As the resident and created electrons have antiparallel spins, the injected exciton can relax to the ground state with a conservation of the spin of both the electron and the hole. This relaxation does not involve an interaction with the Mn spin which is expected to be conserved. This triplet state relaxes to the low-energy $X^- \text{-Mn}$ level $|-5/2, \uparrow_1, \downarrow_1, \uparrow_1\rangle$ without any spin flip and recombines emitting a $\sigma+$ photon (i.e., copolarized with the excitation) on the low-energy line of $X^- \text{-Mn}$ (final state $M = 2$) or at slightly higher energy on a less intense transition towards the level $M = 3$.

For a spin state of the Mn $S_z = +5/2$ and a resident spin-up electron $|\uparrow_1\rangle$, the absorption takes place on the high energy level of the $|\pm 3/2\rangle_T$ bright triplet $|T_0, \uparrow_2, +5/2\rangle$ [Fig. 5(b)]. This state can also relax to $X^- \text{-Mn}$ without any spin flip. It

ends up on the states $|+\frac{5}{2}, \uparrow_1, \downarrow_1, \uparrow_1\rangle$ and produces a copolarized ($\sigma+$) emission on the high-energy line of X^- -Mn.

With an increase in the excitation energy, one successively excites the different spin states of the Mn giving rise to successive copolarized emission on the different X^- -Mn lines starting from the low-energy side to the high-energy side of the X^- -Mn spectra.

Let us now consider that the resident electron is spin down, $|\downarrow_1\rangle$. For a $\sigma+$ excitation which creates an e-h pair $|\downarrow_2, \uparrow_2\rangle$, an absorption cannot occur on the triplet states $|\pm 3/2\rangle_T$ as they do not contain components with parallel electron spins. An absorption can take place at higher energy on the charged exciton states $|+\frac{1}{2}\rangle_{T-}$ associated with the electron triplet T_{-1} .

The exchange interaction with the magnetic atom is still dominated by the antiferromagnetic coupling with the spin-up hole $|\uparrow_2\rangle$, and the lowest energy state that can be excited corresponds to $S_z = -5/2$ [state $|T_{-1}, \uparrow_2, -\frac{5}{2}\rangle$ in Fig. 5(c)]. Now, the resident and created electrons have parallel spins (both are spin down in this case), and the relaxation to X^- from $T_{-1} |\uparrow_2\rangle$ cannot occur directly. The relaxation requires an e-h flip-flop to the state $T_0 |\downarrow_2\rangle$ before relaxing to the X^- singlet state $S_0 |\downarrow_1\rangle$ [18,21]. The Mn spin is not involved in this relaxation process. It is conserved, and the final state after relaxation, $|-\frac{5}{2}, \downarrow_1, \uparrow_1, \downarrow_1\rangle$, has parallel hole and Mn spins. This corresponds to the highest-energy X^- -Mn state, which recombines, emitting a $\sigma-$ photon (i.e., cross-polarized with the resonant excitation) on the high-energy line [Fig. 5(c)].

For a spin state of the Mn $S_z = +5/2$ and a spin-down resident electron $|\downarrow_1\rangle$, a $\sigma+$ excitation creates the state $|T_{-1}, \uparrow_2, +\frac{5}{2}\rangle$, the high energy level associated with the triplet $|+\frac{1}{2}\rangle_T$. Two optical transitions are possible, from $M = 2$ and $M = 3$ [Fig. 5(d)]. An e-h flip-flop is also required for the relaxation toward the low-energy X^- -Mn state $|+\frac{5}{2}, \downarrow_1, \uparrow_1, \downarrow_1\rangle$. It recombines on the two low-energy lines of X^- -Mn emitting a $\sigma-$ photon.

In this case, an increase in the excitation energy gives rise to successive cross-circularly-polarized emission starting from the high-energy line and going to the low-energy line of X^- -Mn PL spectra. This series of cross-circularly-polarized PLE resonances is shifted towards high energy compared with the σ_{co} structure by the isotropic part of the e-h exchange interaction $\tilde{\Delta}^0$.

The series of co-circularly-polarized and cross-circularly-polarized PLE resonances are at the origin of the circularly polarized crosslike structure observed in the PLE spectra of X^- -Mn (Fig. 2). For a given emission line of X^- -Mn, we can assign the observed doublets in the PLE spectra to the excitation of the two bright triplet states of X^{*-} . The relative energy positions of the absorption lines giving rise to the σ_{co} and σ_{cross} PL are controlled both by the e-h exchange interaction $\tilde{\Delta}^0$ and the exchange coupling with the Mn spin.

Calculated PLE spectra of X^- -Mn are presented in Fig. 6. In this model we consider that the QD contains a spin-up electron $|\uparrow_1\rangle$ (identical results are obtained with a spin-down electron by reversing all the circular polarizations). For an estimation of the PLE spectra we also consider that the spin of the Mn and of the resident electron are conserved during the optical transitions and during the relaxation of the optically

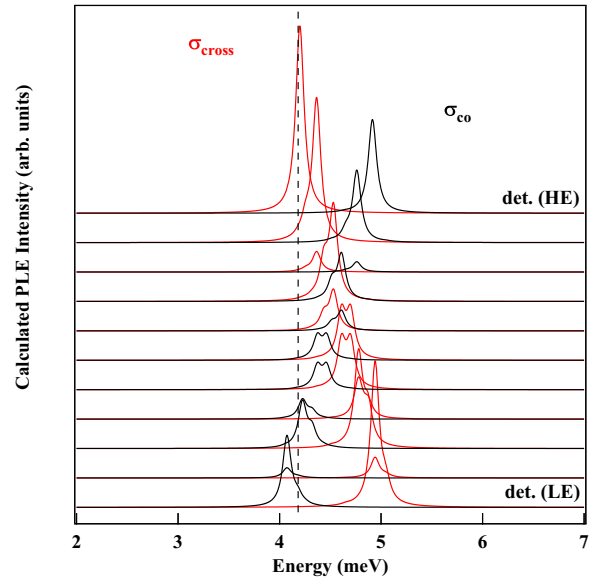


FIG. 6. Calculated PLE spectra of X^- -Mn for a QD containing a spin-up electron $|\uparrow_1\rangle$. PLE spectra of the 11 emission lines of X^- -Mn are displayed for a $\sigma+$ detection and a $\sigma+$ excitation (red) or $\sigma-$ excitation (black). Spectra are shifted for clarity, and a line broadening with a Lorentzian of half width at half maximum of 50 μeV is included. Bottom trace: detection on the low-energy (LE) line. Top trace: detection on the high-energy (HE) line. The parameters used in the calculations are $I_{e_1\text{Mn}} = -30 \mu\text{eV}$, $I_{e_2\text{Mn}} = 0 \mu\text{eV}$, $I_{h_2\text{Mn}} = 100 \mu\text{eV}$, $\tilde{\Delta}^0 = -75 \mu\text{eV}$, $\tilde{\Delta}^1 = 0 \mu\text{eV}$, $\Delta^{ee} = -5000 \mu\text{eV}$, $\rho_s/\Delta_{lh} = 0$, and $\theta_s = 0$. These values reproduce the order of magnitude of the splitting and shift observed on the triplet states in QD1.

created e-h pair from an excited state of the dot to the ground state of the charged exciton.

To obtain the PLE signal, we first calculate the absorption amplitude of the transition between the e-Mn levels in the ground state and each triplet state of the charged exciton in the excited state. The amplitude of transition is calculated in each circular polarization. For instance, for a resident electron with spin up $|\uparrow_1\rangle$, the amplitude of the $\sigma+$ transitions which creates an e-h pair $|\downarrow_2, \uparrow_2\rangle$ is given by the overlap $\langle M, M_z | S_z, \uparrow_1, \downarrow_2, \uparrow_2 \rangle$. This corresponds to an excitation of the triplet state $T_0 |\uparrow_2\rangle$.

For a given line of X^- -Mn, the PL is then given by the product of the intensity of the considered transition $|\langle M, M_z | S_z, \uparrow_1 \rangle|^2$ by the probability of the absorption which creates an excited charged exciton state $|S_z, \uparrow_1, \downarrow_2, \uparrow_2\rangle$ for a $\sigma+$ excitation or $|S_z, \uparrow_1, \uparrow_2, \downarrow_2\rangle$ for a $\sigma-$ excitation. The first one gives rise to a σ_{co} emission, whereas the second one corresponds to a σ_{cross} PL.

In the results presented in Fig. 6 an absorption series with a positive slope (i.e., low-energy excitation gives a PL on the low-energy line, and high-energy excitation gives a PL on the high-energy line) produces a σ_{co} emission, and a second series of absorption with a negative slope, slightly shifted to higher energy, gives rise to σ_{cross} PL. This corresponds to the situation observed in the experiments displayed in Figs. 2 and 3. In the experiments, the broadening of the line prevents the observation of the detailed structure of the calculated

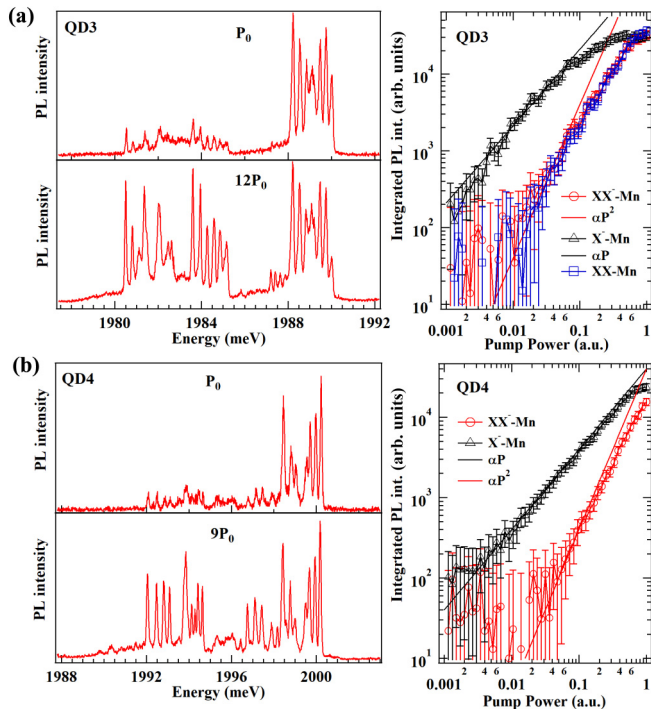


FIG. 7. (a) Excitation power dependence of the PL of QD3 ($E_{\text{ex}} = 2077$ meV) (a) and QD4 ($E_{\text{ex}} = 2074$ meV) (b). Left panels: linearly polarized PL spectra for two excitation powers. Right panels: power dependence of the integrated PL intensity of X^- -Mn and XX^- -Mn (and XX^- -Mn for QD3). Solid lines correspond to linear (black) and quadratic (red) fits. See Fig. 8 for a detailed linear polarization study of QD3 and QD4.

excitation spectra, but a good overall agreement with the model is observed (Fig. 6).

The anisotropic part of the e-h exchange interaction $\tilde{\Delta}^1$ can mix bright triplet states associated with the same Mn spin state. This can introduce some deviation from the purely circularly polarized optical selection rules and induce a perturbation or an energy gap in the center of the absorption structure.

V. NEGATIVELY CHARGED BIEXCITON COUPLED WITH A Mn SPIN

The interaction of the triplet states of X^{*-} with the Mn spin can also be observed in the emission of a negatively charged biexciton. In charged magnetic QDs under high excitation power, additional emission lines appear on the low-energy side of X^- -Mn. The neutral biexciton (XX^- -Mn) is easily identified with its six-line PL structure and its superlinear excitation power dependence [36,37]. However, as presented in Fig. 7 for QD3 and QD4, more complex structures consisting in two groups of lines separated by a central gap can also appear. The groups of lines are partially linearly polarized along two orthogonal directions (Fig. 8). The polarization rate decreases from the center to the outside of the PL structure. The excitation power dependence of the negatively charged exciton is almost linear at low excitation power (Fig. 7). The lowest-energy group of lines appears only at high excitation power, and its dependence on excitation power is almost

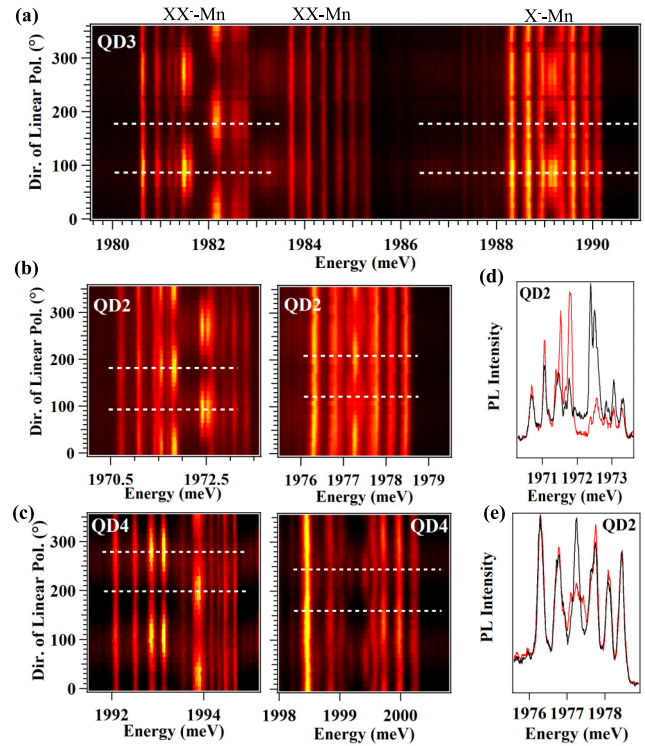


FIG. 8. (a) Linear polarization properties of the PL of X^- -Mn, XX^- -Mn, and XX^- -Mn in QD3 ($E_{\text{ex}} = 2077$ meV). The direction of polarization is measured with respect to the [100] or [010] axis. (b) Linear polarization properties of the PL of XX^- -Mn (left panel) and X^- -Mn (right panel) in QD2 ($E_{\text{ex}} = 2079$ meV). (c) Linear polarization properties of the PL of XX^- -Mn (left panel) and X^- -Mn (right panel) in QD4 ($E_{\text{ex}} = 2074$ meV). (d) and (e) Linearly polarized PL spectra of XX^- -Mn and X^- -Mn, respectively, in QD2 ($E_{\text{ex}} = 2079$ meV). The directions of linear polarization correspond to the dashed lines in (b). In the PL maps, yellow corresponds to a maximum of intensity.

identical to that observed for the biexciton and is superlinear (Fig. 7).

This PL structure corresponds to a recombination of a negatively charged biexciton interacting with the magnetic atom (XX^- -Mn). XX^- consists of two holes and three electrons [27,38]. Within this complex, the total angular momentum of the two holes and the total spin of the two electrons which are in the lowest energy state of the dot are zero. XX^- is then twice degenerate with respect to the spin of the third electron ($|\uparrow_1\rangle$ or $|\downarrow_1\rangle$) occupying an excited state of the dot.

The PL of XX^- arises from the recombination of an e-h pair in the lowest energy level of the dot. An excited charged exciton with an electron in an excited state and an e-h pair in the lowest energy state is left behind as the final state of the radiative recombination (Fig. 9). This excited charged exciton is different from the one created by a resonant excitation on an excited state as now the hole is in the lowest energy state of the QD. It is, however, similarly split into a high-energy singlet and a lower-energy triplet by the e-e exchange interaction. The triplet states are also split by the e-h exchange interaction. The e-e exchange interaction involves an electron in the lowest energy state and one in an excited state and is identical to the one we discussed for the PLE of X^- -Mn. The exchange

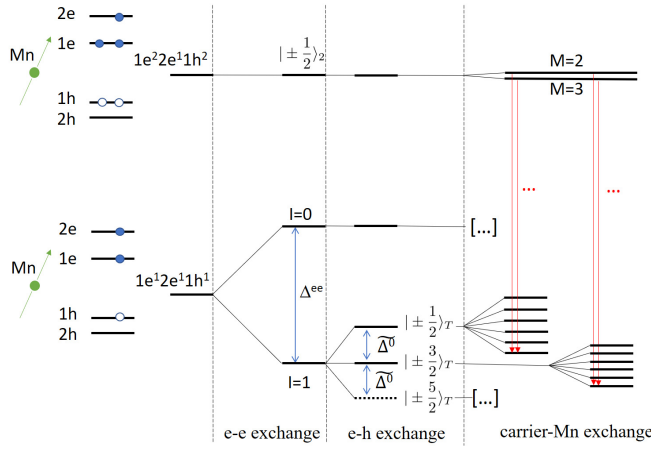


FIG. 9. Scheme of the energy levels of the initial and final states in the optical recombination of a negatively charged biexciton in a Mn-doped QD.

interaction of the electron with the hole which is now confined on the lowest energy state of the dot is expected to be larger than the one observed for the resonantly excited X^{-*} (Sec. IV) where the hole is less confined on an excited state.

In nonmagnetic QDs, the recombination of XX^{-} towards the two bright triplet states of X^{-*} gives rise to a PL doublet split by the e-h exchange interaction $\tilde{\Delta}^0$ [27]. In the presence of an anisotropic confinement potential, these optically active triplet states are coupled by the energy $\tilde{\Delta}^1$ and become partially linearly polarized.

In a magnetic QD, the spin of the electron in the excited state, $\vec{\sigma}_2$, is exchange coupled with the spin of the magnetic atom \vec{S} (Fig. 9). As in the case of X^{-} -Mn described in Sec. III, the isotropic coupling between the electron spin $1/2$ and the spin $5/2$ of the atom should result in two energy levels with total angular momentum $M = 2$ and $M = 3$. The splitting is controlled by the exchange interaction of the electron in the excited state with the Mn spin, I_{e_2Mn} . Because of the weaker confinement in the excited state, a value $I_{e_2Mn} < I_{e_1Mn}$ is expected.

A. Polarized fine structure of the negatively charged biexciton

In the final state of the optical recombination of XX^{-} -Mn, each triplet state of X^{-*} -Mn interacts through the exchange interaction with the Mn atom. This interaction is dominated by the antiferromagnetic coupling with the heavy hole in the QD ground state and, for each triplet state, results in a splitting into six energy levels. The energy shift induced by this exchange interaction competes with the anisotropic exchange interaction term $\tilde{\Delta}^1$. $\tilde{\Delta}^1$ mixes the two bright triplet states and can induce a gap in the center of the PL structure and a linear polarization rate.

The presence of the magnetic atom permits us to independently observe two sources of anisotropy: the VBM responsible for the linear polarization in the center of X^{-} -Mn and the long-range exchange interaction in an anisotropic potential responsible for the linear polarization of XX^{-} -Mn. As revealed by the polarization map presented in Fig. 8 for QD2, QD3, and QD4, the directions of linear polarization observed

for the two charged complexes are in general not identical. The direction of polarization is measured with respect to the [100] or [010] axis of the sample (i.e., at 45° from the easy cleavage axis of the substrate). In the investigated QDs, the directions of polarization for XX^{-} -Mn are roughly aligned with the [100] or [010] axis. The directions of linear polarization of X^{-} -Mn are more fluctuating. They can be aligned with the direction of linear polarization of XX^{-} -Mn as in QD3, along the [110] axis as in QD4, or at an intermediate angle (around 30° in QD2). This directly shows that the shape anisotropy responsible for linear polarization of XX^{-} -Mn and the strain anisotropy responsible for the linear polarization of X^{-} -Mn are independent in these self-assembled QDs.

To analyze in more detail the emission of XX^{-} -Mn, we use a spin effective model. In the initial state, XX^{-} -Mn can be split by the weak electron-Mn exchange interaction $I_{e_2Mn}\vec{\sigma}_2\vec{S}$. In the final state, the triplets of X^{-*} are split by the e-h exchange interaction

$$H_{e_1e_2h_1} = 2\tilde{\Delta}^0 I_z \sigma_z^h + \tilde{\Delta}^1 (I_x \sigma_x^h + I_y \sigma_y^h). \quad (5)$$

The exchange constants $\tilde{\Delta}^{0,1}$ differ from the ones discussed for the resonant excitation of X^{-*} -Mn where the hole is weakly confined on an excited state of the dot. In the final state of the XX^{-} recombination, the hole is more strongly confined on the lowest energy state of the dot. One can expect a larger exchange interaction with the electron resulting in a larger splitting of the triplet and a stronger influence of a possible shape anisotropy.

The triplet states are further coupled with the Mn atom, and the X^{-*} -Mn Hamiltonian reads

$$H_{X^{-*}-Mn} = H_{e_1e_2h_1} + I_{e_1Mn}\vec{\sigma}_1\vec{S} + I_{e_2Mn}\vec{\sigma}_2\vec{S} + I_{h_1Mn}\vec{J}_1\vec{S}. \quad (6)$$

Under nonresonant optical excitation, the injected e-h pair is not spin polarized, and all the XX^{-} -Mn states, weakly split by the e-Mn exchange interaction, are populated with equal probabilities. The emission spectra can be obtained by calculating the overlap of the initial e-Mn states $\langle M, M_z |$ with each of the triplet levels in the final state of the transition, $|T_{\mp 1}, J_{z_1} = \pm \frac{3}{2}, S_z\rangle$, $|T_0, J_{z_1} = \pm \frac{3}{2}, S_z\rangle$, and $|T_{\pm 1}, J_{z_1} = \pm \frac{3}{2}, S_z\rangle$. However, transitions towards the dark triplets $|T_{\pm 1}, J_{z_1} = \pm \frac{3}{2}, S_z\rangle$ are forbidden. For a $\sigma+$ recombination, for instance, the intensities of the optically active transitions are given by $|\langle M, M_z | T_{+1}, J_{z_1} = -\frac{3}{2}, S_z \rangle|^2$ and $|\langle M, M_z | T_0, J_{z_1} = -\frac{3}{2}, S_z \rangle|^2$.

Results of a modeling of the PL of XX^{-} -Mn are presented in Fig. 10. In this model, $\tilde{\Delta}^0$ controls the splitting between the two groups of lines. The long-range exchange coupling term $\tilde{\Delta}^1$ controls the central gap and the linear polarization rate. $\tilde{\Delta}^1$ is chosen to be real meaning that the shape anisotropy is oriented along the [100] axis. The main feature of the emission spectra and their linear polarization dependence can be reproduced by the spin effective model. A good agreement can be obtained neglecting the exchange interaction of the magnetic atom with the electron spin in the excited state of the dot. As will be confirmed by magneto-optic measurements, a VBM induced by in-plane strain anisotropy can produce an additional small gap on the high-energy side of the spectra [circle in Fig. 11(e)].

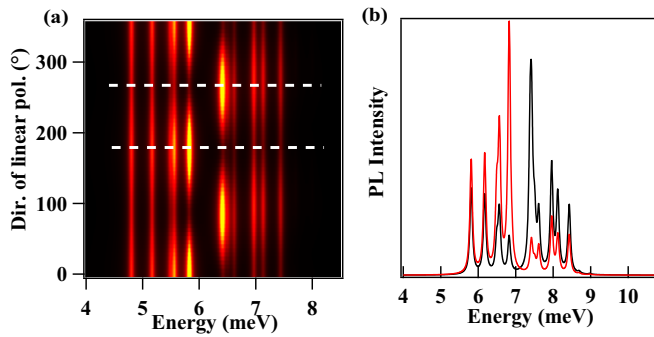


FIG. 10. Model of the linear polarization properties of XX^- -Mn. The direction of linear polarization is indicated with respect to the $[100]$ axis. (a) Intensity map of the linearly polarized PL. (b) PL spectra along two orthogonal directions indicated by dashed lines in (a). Calculations were performed with $I_{e_1Mn} = -70 \mu\text{eV}$, $I_{e_2Mn} = 0 \mu\text{eV}$, $I_{h_1Mn} = 230 \mu\text{eV}$, $\tilde{\Delta}^0 = -700 \mu\text{eV}$, $\Delta_{ee} = -5000 \mu\text{eV}$, $\tilde{\Delta}_1 = 350 \mu\text{eV}$, $\rho_s/\Delta_{th} = 0.2$, $\theta_s = \pi/4$, and $\xi = 0.15$. These values reproduce the order of magnitude of the splittings observed for XX^- -Mn in QD2 or QD4. A line broadening with a Lorentzian of half width at half maximum of $50 \mu\text{eV}$ is included. In the PL map, yellow corresponds to a maximum of intensity.

B. Magneto-optical properties of the negatively charged biexciton

The observation of the evolution of the emission of XX^- -Mn under magnetic field permits us to probe the magneto-optic properties of the charged exciton triplets interacting with the magnetic atom. The magnetic field dependence of different charged excitonic complexes is presented in Fig. 11 for QD2, QD3, and QD4.

For XX^- -Mn, the energy gap induced by $\tilde{\Delta}^1$ which is almost at the center of the emission structure at zero magnetic field evolves towards the low-energy side in $\sigma+$ polarization and towards the high-energy side in $\sigma-$ polarization. Some anticrossings are usually observed at weak magnetic field (in the range 2–3 T) in $\sigma+$ polarization [see detailed weak-field scan of QD2 and QD4 in Figs. 11(d) and 11(e)]. The width of the central gap slightly decreases when a longitudinal magnetic field is applied. This is particularly clear between 0 and 5 T.

The overall behavior of the magnetic field dependence can be reproduced by a spin effective model (Fig. 12). For this model, Zeeman energies of the carriers and magnetic atom spins, $g_i \mu_B \vec{S}_i \cdot \vec{B}$, are included in the zero-field spin Hamiltonian (6). A diamagnetic shift of the excitonic complex γB^2 is also added. The electron-Mn coupling in the initial state, I_{e_2Mn} , is neglected as a value larger than a few tens of μeV would produce anticrossings in the low-magnetic-field region which are not resolved in the experimental spectra.

The series of anticrossings observed in the low-magnetic-field region around 2–3 T in $\sigma+$ polarization can also be reproduced by the model [Fig. 12(b)]. Similar perturbations are observed for X^- -Mn but on $\sigma-$ polarized lines which shift towards low energy under a positive magnetic field [see highlighted area in Figs. 11(f) and 11(g)]. This is the opposite in the XX^- -Mn case.

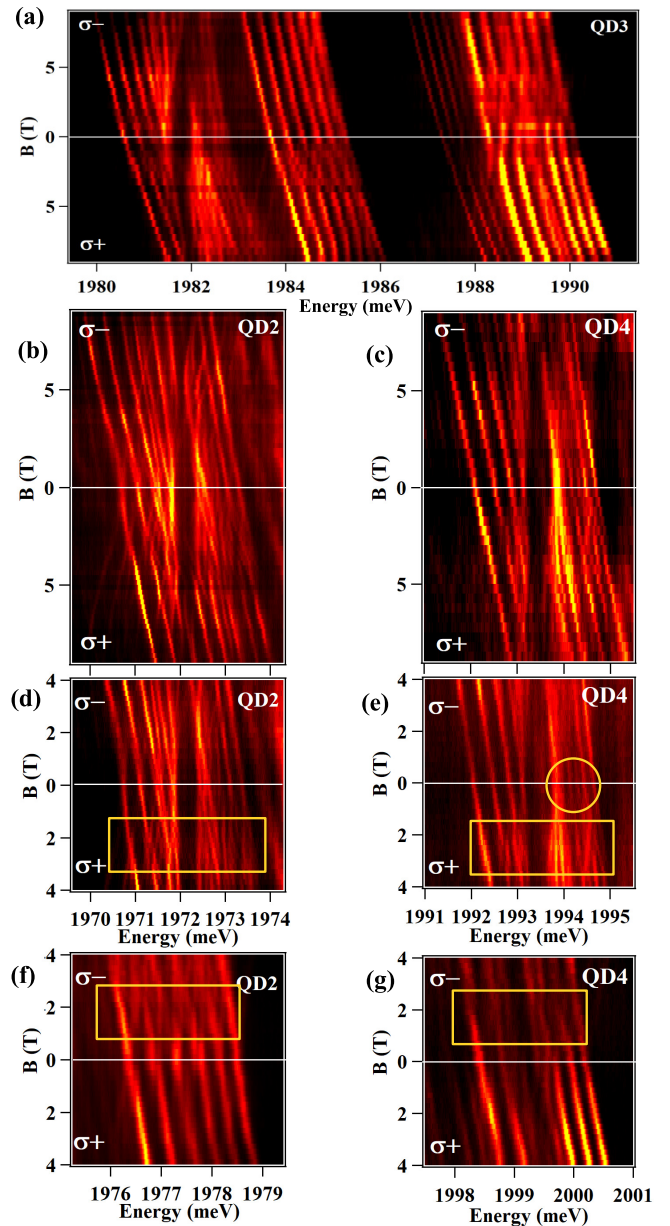


FIG. 11. PL intensity map of the longitudinal magnetic field dependence of QD2 ($E_{\text{ex}} = 2079 \text{ meV}$), QD3 ($E_{\text{ex}} = 2077 \text{ meV}$), and QD4 ($E_{\text{ex}} = 2074 \text{ meV}$). (a) Magnetic field dependence of X^- -Mn, XX^- -Mn, and XX^- -Mn in QD3. (b) and (c) Magnetic field dependence of XX^- -Mn in QD2 and QD4, respectively. (d) and (e) Detail of the low-field dependence of XX^- -Mn in QD2 and QD4, respectively. (f) and (g) Detail of the low-field dependence of X^- -Mn in QD2 and QD4, respectively. In (d)–(g) the rectangles highlight regions where anticrossings take place. In (e), a circle highlights weak perturbations induced by VBM. Yellow corresponds to a maximum of intensity.

The mixing of these levels arises from a VBM induced by shear strain. As in the case of in-plane strain anisotropy, such a VBM can be described by effective spin operators acting on the heavy-hole subspace $\tilde{j}_+ = \xi\sqrt{3}\tau_z$, $\tilde{j}_- = \xi^*\sqrt{3}\tau_z$, and $\tilde{j}_z = 3/2\tau_z$ [33]. The mixing occurs in the initial state of the optical transition for X^- -Mn when the Zeeman energy of the Mn compensates the hole-Mn exchange interaction and

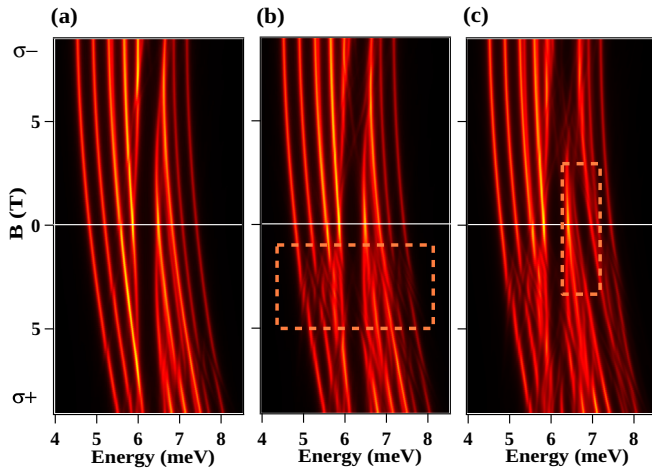


FIG. 12. (a) Longitudinal magnetic field dependence of the PL intensity of a XX^- -Mn calculated with the following parameters: (a) $I_{e_1Mn} = -70 \mu\text{eV}$, $I_{e_2Mn} = 0 \mu\text{eV}$, $I_{h_1Mn} = 230 \mu\text{eV}$, $\tilde{\Delta}_0 = -700 \mu\text{eV}$, $\tilde{\Delta}^1 = 350 \mu\text{eV}$, $\Delta_{ee} = -5000 \mu\text{eV}$, $\rho_s/\Delta_{lh} = 0$, $\theta_s = \pi/4$, $\xi = 0$, $g_{e1} = -0.4$, $g_{e2} = -0.4$, $g_h = 0.5$, $g_{Mn} = 2$, and $\gamma = 2.5 \mu\text{eV/T}^2$. (b) Same as (a), but with $\xi = 0.15$. (c) Same as (a), but with $\xi = 0.15$ and $\rho_s/\Delta_{lh} = 0.2$. A line broadening with a Lorentzian of half width at half maximum of $50 \mu\text{eV}$ is included. Yellow corresponds to a maximum of intensity.

hole-Mn levels overlap. The same thing occurs in the final state of the transition in the case of the XX^- -Mn when the Zeeman energy of the Mn compensates the bright-exciton-Mn exchange splitting (the electron-Mn exchange interaction in the excited state can be neglected).

A perturbation of the spectra in the form of a small gap can appear on the high-energy side of the XX^- -Mn spectra in some of the dots. As shown by the result of the model presented in Fig. 12(c), it is produced by the presence of VBM induced by in-plane strain anisotropy.

The slight decrease in the width of the central gap observed at large magnetic field is not reproduced by the model. It likely corresponds to a decrease in the anisotropic part of the e-h exchange interaction with the increase in a longitudinal magnetic field. A similar reduction of the e-h exchange interaction was already observed in the magneto-PL of a doubly charged exciton coupled with a Mn [39]. This decrease can be induced by a decrease in the anisotropy of the wave function in the excited state under a longitudinal magnetic field which cannot be described by a spin effective model.

As presented in Fig. 13(a), under a magnetic field applied in the plane of the QD (transverse magnetic field), each PL line of XX^- -Mn splits into multiplets. These splittings result from a mixing of the Mn spin states by the transverse magnetic field. As the Mn levels within XX^- -Mn are only weakly coupled with the electron, a weak transverse field splits the magnetic atom spin states. They are then quantized in the QD plane along the direction of the applied magnetic field, x .

In the final state, the Mn atom is exchange coupled with the e-h pair confined in the lowest energy state of the QD. We can then define an effective quantization axis for the Mn spin, the A axis, orientated along the sum of applied and exchange fields. As observed for neutral and singly charged excitons

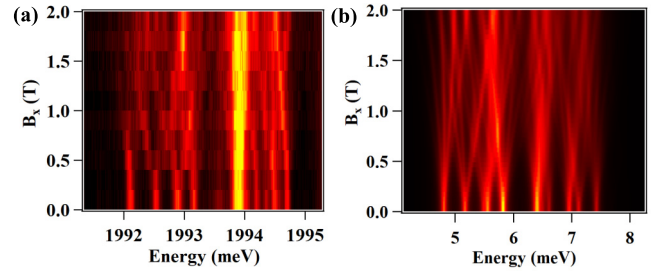


FIG. 13. (a) Transverse magnetic field dependence of the PL of XX^- -Mn in QD4 ($E_{ex} = 2074 \text{ meV}$). The magnetic field is applied along the [100] or [010] axis. (b) Model of the transverse magnetic field dependence of XX^- -Mn calculated with the same parameters as for Fig 12(c) and a magnetic field applied along the [100] axis. A line broadening with a Lorentzian of half width at half maximum of $50 \mu\text{eV}$ is included. Yellow corresponds to a maximum of intensity.

[6,24], at low applied transverse field the effective field is dominated by exchange interaction with the hole quantized along the QD growth axis z . During the optical recombination, the Mn spin has to pass from an eigenstate of S_x to an eigenstate of S_A . A system with spin S prepared with a spin projection S_x along x can be measured to have any of the projections S_A along A with probabilities given by the rotation matrix of a spin S . Each XX^- -Mn state associated with a given S_x Mn spin can then recombine on any of the S_A final X^* -Mn spin states, except when the two quantization axes are identical. As reproduced by the model presented in Fig. 13(b), this increases the number of emission lines, and each transition observed at zero field splits in a large fan.

VI. CONCLUSION

To conclude, we examined two ways to probe the exchange interaction of the triplet states of an excited negatively charged exciton with the spin of an individual magnetic atom (Mn) in a QD: the direct excitation of the excited states of X^- -Mn and the detection of the PL of XX^- -Mn.

The excitation of the triplet state of a charged exciton reveals that the negative circular polarization is conserved in the presence of the magnetic atom. This shows that in the investigated QDs, despite the exchange coupling with the magnetic atom, the spin relaxation of the electron triplets remains dominated by the e-h exchange interaction. The emission of XX^- -Mn permits us to observe independently the isotropic and anisotropic parts of the e-h exchange interaction and to analyze the magneto-optic properties of charged exciton triplets coupled with a magnetic atom.

The resonant initialization of excitonic states in the high-energy orbital levels of QDs provides additional degrees of freedom for optical spin control protocols [40]. Resonant excitation of charged exciton triplet states permits us to efficiently inject spin-polarized electrons in a charged QD. This could be used in future work to probe the magnetic field dependence of the spin dynamics of an electron-Mn complex or to control the coupling between two magnetic atoms in the same QD through their interaction with a spin-polarized electron [41,42].

- [1] C. T. Nguyen, D. D. Sukachev, M. K. Bhaskar, B. Machielse, D. S. Levonian, E. N. Knall, P. Stroganov, R. Riedinger, H. Park, M. Loncar, and M. D. Lukin, *Phys. Rev. Lett.* **123**, 183602 (2019).
- [2] S. Wein, J. Loredó, M. Maffei, P. Hilaire, A. Harouri, N. Somaschi, A. Lemaître, I. Sagnes, L. Lanco, O. Krebs, A. Auffèves, C. Simon, P. Senellart, and C. Antón-Solanas, *Nat. Photonics* **16**, 374 (2022).
- [3] L. M. K. Vandersypen, H. Bluhm, J. S. Clarke, A. S. Dzurak, R. Ishihara, A. Morello, D. J. Reilly, L. R. Schreiber, and M. Veldhorst, *npj Quantum Inf.* **3**, 34 (2017).
- [4] M. F. Gonzalez-Zalba, S. de Franceschi, E. Charbon, T. Meunier, M. Vinet, and A. S. Dzurak, *Nat. Electron.* **4**, 872 (2021).
- [5] L. Besombes, Y. Leger, L. Maingault, D. Ferrand, H. Mariette, and J. Cibert, *Phys. Rev. Lett.* **93**, 207403 (2004).
- [6] Y. Leger, L. Besombes, L. Maingault, D. Ferrand, and H. Mariette, *Phys. Rev. B* **72**, 241309(R) (2005).
- [7] A. Kudelski, A. Lemaître, A. Miard, P. Voisin, T. C. M. Graham, R. J. Warburton, and O. Krebs, *Phys. Rev. Lett.* **99**, 247209 (2007).
- [8] A. K. Bhattacharjee, *Phys. Rev. B* **76**, 075305 (2007).
- [9] L. Besombes, Y. Leger, J. Bernos, H. Boukari, H. Mariette, J. P. Poizat, T. Clement, J. Fernández-Rossier, and R. Aguado, *Phys. Rev. B* **78**, 125324 (2008).
- [10] C. Le Gall, R. S. Kolodka, C. L. Cao, H. Boukari, H. Mariette, J. Fernández-Rossier, and L. Besombes, *Phys. Rev. B* **81**, 245315 (2010).
- [11] L. Besombes and H. Boukari, *Phys. Rev. B* **89**, 085315 (2014).
- [12] J. Kobak, T. Smolenski, M. Goryca, M. Papaj, K. Gietka, A. Bogucki, M. Koperski, J.-G. Rousset, J. Suffczynski, E. Janik, M. Nawrocki, A. Golnik, P. Kossacki, and W. Pacuski, *Nat. Commun.* **5**, 3191 (2014).
- [13] T. Smolenski, T. K. J. Kobak, M. Goryca, A. Golnik, P. Kossacki, and W. Pacuski, *Nat. Commun.* **7**, 10484 (2016).
- [14] A. Lafuente-Sampietro, H. Utsumi, H. Boukari, S. Kuroda, and L. Besombes, *Phys. Rev. B* **93**, 161301(R) (2016).
- [15] T. Flissikowski, A. Hundt, M. Lowisch, M. Rabe, and F. Henneberger, *Phys. Rev. Lett.* **86**, 3172 (2001).
- [16] R. Dzhioev, B. Zakharchenya, V. Korenev, P. Pak, D. Vinokurov, O. Kovalenkov, and I. Tarasov, *Phys. Solid State* **40**, 1587 (1998).
- [17] R. Dzhioev, B. Zakharchenya, V. Korenev, and M. Lazarev, *Phys. Solid State* **41**, 2014 (1999).
- [18] O. Cortez, O. Krebs, S. Laurent, M. Senes, X. Marie, P. Voisin, R. Ferreira, G. Bastard, J.-M. Gérard, and T. Amand, *Phys. Rev. Lett.* **89**, 207401 (2002).
- [19] M. E. Ware, E. A. Stinaff, D. Gammon, M. F. Doty, A. S. Bracker, D. Gershoni, V. L. Korenev, S. C. Badescu, Y. Lyanda-Geller, and T. L. Reinecke, *Phys. Rev. Lett.* **95**, 177403 (2005).
- [20] B. Eble, O. Krebs, A. Lemaître, K. Kowalik, A. Kudelski, P. Voisin, B. Urbaszek, X. Marie, and T. Amand, *Phys. Rev. B* **74**, 081306(R) (2006).
- [21] C. Le Gall, A. Brunetti, H. Boukari, and L. Besombes, *Phys. Rev. B* **85**, 195312 (2012).
- [22] J. K. Furdyna, *J. Appl. Phys.* **64**, R29 (1988).
- [23] Y. Leger, L. Besombes, J. Fernandez-Rossier, L. Maingault, and H. Mariette, *Phys. Rev. Lett.* **97**, 107401 (2006).
- [24] L. Besombes, Y. Léger, L. Maingault, and H. Mariette, *J. Appl. Phys.* **101**, 081713 (2007).
- [25] B. Varghese, H. Boukari, and L. Besombes, *Phys. Rev. B* **90**, 115307 (2014).
- [26] A. Lafuente-Sampietro, H. Boukari, and L. Besombes, *Phys. Rev. B* **92**, 081305(R) (2015).
- [27] I. A. Akimov, K. V. Kavokin, A. Hundt, and F. Henneberger, *Phys. Rev. B* **71**, 075326 (2005).
- [28] B. Urbaszek, R. J. Warburton, K. Karrai, B. D. Gerardot, P. M. Petroff, and J. M. Garcia, *Phys. Rev. Lett.* **90**, 247403 (2003).
- [29] K. V. Kavokin, *Phys. Status Solidi A* **195**, 592 (2003).
- [30] A. C. Johnson, J. R. Petta, C. M. Marcus, M. P. Hanson, and A. C. Gossard, *Phys. Rev. B* **72**, 165308 (2005).
- [31] P. Wojnar, C. Bougerol, E. Bellet-Amalric, L. Besombes, H. Mariette, and H. Boukari, *J. Cryst. Growth* **335**, 28 (2011).
- [32] Y. Leger, L. Besombes, L. Maingault, and H. Mariette, *Phys. Rev. B* **76**, 045331 (2007).
- [33] V. Tiwari, M. Arino, S. Gupta, M. Morita, T. Inoue, D. Caliste, P. Pochet, H. Boukari, S. Kuroda, and L. Besombes, *Phys. Rev. B* **104**, L041301 (2021).
- [34] L. C. Lew Yan Voon and M. Willatzen, *The $k \cdot p$ Method* (Springer, Berlin, 2009).
- [35] M. Bayer, G. Ortner, O. Stern, A. Kuther, A. A. Gorbunov, A. Forchel, P. Hawrylak, S. Fafard, K. Hinzer, T. L. Reinecke, S. N. Walck, J. P. Reithmaier, F. Klopff, and F. Schafer, *Phys. Rev. B* **65**, 195315 (2002).
- [36] L. Besombes, Y. Leger, L. Maingault, D. Ferrand, H. Mariette, and J. Cibert, *Phys. Rev. B* **71**, 161307(R) (2005).
- [37] A. H. Trojnar, M. Korkusinski, E. S. Kadantsev, P. Hawrylak, M. Goryca, T. Kazimierczuk, P. Kossacki, P. Wojnar, and M. Potemski, *Phys. Rev. Lett.* **107**, 207403 (2011).
- [38] J. Kettler, M. Paul, F. Olbrich, K. Zeuner, M. Jetter, P. Michler, M. Florian, C. Carmesin, and F. Jahnke, *Phys. Rev. B* **94**, 045303 (2016).
- [39] T. Smolenski, M. Koperski, M. Goryca, P. Wojnar, P. Kossacki, and T. Kazimierczuk, *Phys. Rev. B* **92**, 085415 (2015).
- [40] S. Germanis, P. Atkinson, A. Bach, R. Hostein, R. Braive, M. Vabre, F. Margaillan, M. Bernard, V. Voliotis, and B. Eble, *Phys. Rev. B* **105**, 235430 (2022).
- [41] L. Besombes, C. L. Cao, S. Jamet, H. Boukari, and J. Fernandez-Rossier, *Phys. Rev. B* **86**, 165306 (2012).
- [42] O. Krebs and A. Lemaître, *Phys. Rev. Lett.* **111**, 187401 (2013).